UCAs DoA with Reduced Number of Sensors and Small Sample Support via Beamspace Harmonics Decomposition and Root-MUSIC Algorithm

Guilherme Ferreira Murmel Liali[1]
[1]Centro de Guerra Acústica e Eletrônica da Marinha, Niterói/Rio de Janeiro - Brasil

***Abstract*— In this work, we evaluate a Uniform Circular Array, featuring a reduced number of sensors and using small sample support comprised of only a few snapshots, for 2-D DoA estimation. Phase-mode transformation is a harmonics decomposition that allows the use of Root-MUSIC algorithm for azimuth estimation. Next, we address the challenging issues of having an insufficient number of sensors in the array and limited sample support, followed by a brief discussion of the techniques that can be used to mitigate the degradation caused by the two aforementioned limitations. Several numerical simulations are conducted to evaluate the DoA estimation performance of narrowband acoustic signals in different scenarios, having water as propagating media. Both isolated and joint effects of the limiting factors, as well as a simulated underwater environment.**

***Keywords*— Uniform Circular Array, Phase-mode Transformation, Small Sample Support.**

I. Introduction

Uniform Circular Arrays (UCAs) are capable of 2-D Direction of Arrival (DoA) estimation, having omnidirectional beampattern with isotropic azimuth properties [1]. These characteristics suit brandband sonar arrays, Radar and Communications Electronic Warfare Support Measures (RESM/CESM) systems, 5G smart antennas, and secure directional communications. However, some essential array signal processing techniques cannot be applied due to the particular form of the array manifold vector [2]–[4], notably the Root-MUSIC algorithm for DoA estimation.

This limitation can be circumvented via beamspace transform based on harmonics, or phase mode, excitation [5], [6], allowing the Root-MUSIC algorithm to be used. The number of harmonics or phase modes depends on spatial sampling and should produce an accurate description of the receiving characteristics of the array in beamspace, otherwise resulting in biased DoA estimations [7].

Root-MUSIC can be paired with reduced sample support for the DoA solution, in which case, reasonable estimates of the covariance matrix are unattainable [8]. Nevertheless, several techniques can emulate the effects of the temporal averaging present in a large number of snapshots. The conditioning of the sample covariance matrix to a known ideal Toeplitz structure can mitigate the undesired effects.

This paper focuses on analyzing UCA uncoupled 2-D DoA estimation in element-space and beamspace, employing combined techniques to tackle the issues of small sample support and a reduced number of sensors. Performance regarding several parameters is evaluated in experiments of gradually increasing complexity. Given that the phase-mode transformation alters a portion of the array manifold as a function of the azimuthal angle, most beamspace UCA works focus only on 1-D Azimuth DoA.

In addition to the usual assessment of the non-isotropic behavior of the zenithal angle ($90°-$ elevation angle) estimation, this work uses a set of computer experiments, simulating air, and underwater narrow-band sound propagation, to analyze the performance regarding the effects of incorporating phase modes into UCAs featuring a reduced number of sensors, as well as the implications of small sample support. Specifically, we assess the effects on the performance of the DoA estimation with and without contingency methods when dealing with a reduced number of sensors and snapshots. The contributions in this work are related to UCA DoA estimation specifically in two dimensions using the Root-MUSIC algorithm with a uniform circular array, subject to a limited number of snapshots and sensors.

This paper is structured as follows. Section II discusses beamspace DoA Estimation and the UCA signal model. Sections III and IV deal with limited spatial and temporal sampling, respectively. Finally, simulation results are addressed in Section V followed by conclusion and final remarks in Section VI.

II. Beamspace DoA Estimation

A. Element-space and Beamspace Signal Models

Consider a UCA with radius R and M sensors in the absence of mutual coupling, as depicted in Fig. 1. With D

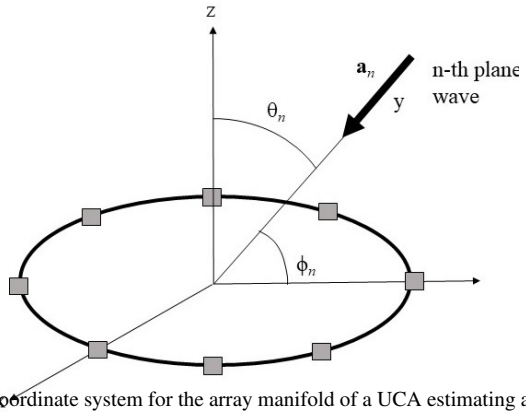

Fig. 1. Coordinate system for the array manifold of a UCA estimating azimuth (ϕ_n) and zenith (θ_n) of a n-th plane wave hitting the array.

emitters and uncorrelated isotropic noise, we may express the snapshot as follows.

$$\mathbf{x}(k) = \mathbf{A}\mathbf{s}(k) + \mathbf{n}(k), \tag{1}$$

where $\mathbf{A} = \begin{bmatrix} \mathbf{a}(\phi_1, \theta_1) & \cdots & \mathbf{a}(\phi_D, \theta_D) \end{bmatrix}$ is the $M \times D$ array manifold matrix, $\mathbf{s}(k)$ is the $D \times 1$ signal vector hitting

the center of the array and $\mathbf{n}(k) = \begin{bmatrix} n_1(k) & \cdots & n_M(k) \end{bmatrix}^{\mathrm{T}}$ is the $M \times 1$ noise vector. The element-space covariance matrix is then given as

$$\mathbf{R}_x = \mathrm{E}[\mathbf{x}(k)\mathbf{x}^{\mathrm{H}}(k)] = \mathbf{A}\mathbf{R}_s\mathbf{A}^{\mathrm{H}} + \sigma_n^2\mathbf{I}_M, \tag{2}$$

where $\mathbf{R}_s$ is the covariance matrix of the input signals and $\sigma_n^2\mathbf{I}_M$ the covariance matrix of the noise signal, σ_n^2 being the noise variance and $\mathbf{I}_M$ the $M \times M$ identity matrix.

The element space array manifold vector with azimuth ϕ, considering a given zenithal angle θ, is

$$\mathbf{a}(\phi) = [e^{\mathrm{j}Y\bar{R}\cos(\phi)}, e^{\mathrm{j}Y\bar{R}\cos(\phi-\frac{2\pi}{M})} \ldots e^{\mathrm{j}Y\bar{R}\cos(\phi-\frac{2\pi(M-1)}{M})}]^{\mathrm{T}}, \tag{3}$$

where $Y = 2\pi/\lambda$ is the wavenumber and $\bar{R} = R\sin\theta$. Not having a Vandermonde structure, $\mathbf{a}(\phi)$ is not convenient for using ROOT-MUSIC algorithm [9]. References [10]–[12] employ harmonics excitation to overcome this limitation and avoid an expensive 2-D grid search exploiting the equivalence between spacial sampling and DFT of the output signal of the circular aperture.

Through N-point DFT of the periodic output of the sampled aperture and applying the Jacobi-Anger expansion [13] $\mathrm{e}^{x\cos(\phi)} = \sum_{q=-\infty}^{\infty} \mathrm{j}^q J_q(x)\mathrm{e}^{\mathrm{j}q\phi}$, each phase mode $\bar{x}_n(k)$ of the beamspace array signal output $\bar{\mathbf{x}}(k)$ is then given by

$$\bar{x}_n(k) = s(k)\frac{1}{\sqrt{M}} \sum_{q=-\infty}^{\infty} j^q J_q\left(Y\bar{R}\right) \mathrm{e}^{\mathrm{j}q\phi} \sum_{m=0}^{M-1} \mathrm{e}^{\frac{-j2\pi qm}{M}} \mathrm{e}^{\frac{j2\pi nm}{M}}, \tag{4}$$

where $J_q(.)$ is the Bessel function of the first kind and order q. In the following, we apply several simplifications to Eq. (4).

As in [14], analysing the inner summation in (4) leads to

$$\sum_{m=0}^{M-1} e^{-j2\pi qm/M} e^{j2\pi nm/M} = \begin{cases} M, & \text{if } q = n + lM, l \in \mathbb{Z}, \\ 0, & \text{otherwise.} \end{cases} \tag{5}$$

Applying additional simplifications as in [11], [15] to Eq. (4), and considering the behavior of the Bessel functions depicted in Fig. 2, we obtain

$$\begin{aligned} \bar{x}_n(k) &\approx s(k)\sqrt{M} \sum_{l=-\infty}^{\infty} j^{n\pm lM} J_{n\pm lM}\left(Y\bar{R}\right) \mathrm{e}^{(j(n\pm lM)\phi)} \\ &\approx s(k)\sqrt{M}\left[j^n J_n\left(Y\bar{R}\right)\mathrm{e}^{(jn\phi)}\right. \\ &\sum_{l=1}^{\infty}\left(j^{n+lM} J_{n+lM}\left(Y\bar{R}\right)\mathrm{e}^{(j(n+lM)\phi)}\right. \\ &\left.\left. + j^{n-lM} J_{n-lM}\left(Y\bar{R}\right)\mathrm{e}^{(j(n-lM)\phi)}\right)\right]. \end{aligned} \tag{6}$$

Considering $l = 0$, we can express $\bar{x}_n(k)$ as a single term:

$$\bar{x}_n(k) \approx s(k)\sqrt{M}\mathrm{j}^n J_n\left(Y\bar{R}\right)\mathrm{e}^{\mathrm{j}n\phi}, -N \le n \le N, \tag{7}$$

where $N = \lfloor (M-1)/2 \rfloor$ denotes the largest integer smaller than or equal to $(M-1)/2$. Eq. (7) defines the entries of $\bar{\mathbf{x}}(k)$ and also its dimensions from the number of phase modes involved in the beamspace transformation. Through this formulation, we manage to transform the $M \times 1$ vector $\mathbf{x}(k)$ into the $(2N+1)\times 1$ $\bar{\mathbf{x}}(k)$ vector with $2N+1 \le M$, for M odd, or $2N+1 \le M-1$, for M even. The beamforming matrix for a given N, defined as $\mathbf{W} = [\mathbf{w}_{-N} \cdots \mathbf{w}_{-1}\ \mathbf{w}_0\ \mathbf{w}_1 \cdots \mathbf{w}_N]$,

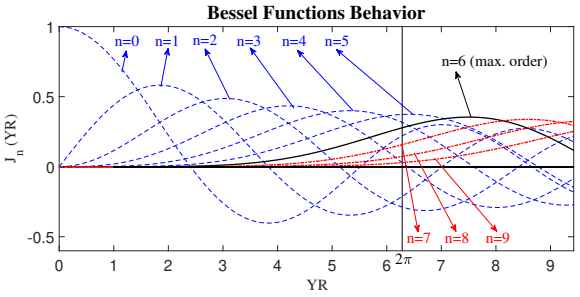

Fig. 2. Behavior of the Bessel functions and dependence on the zenith parameter θ. The blue dashed curves are Bessel functions of the first kind of order 0 to 5, in which the order n is smaller than the maximum argument 2π. The black curve is the Bessel function of the highest order less than the maximum argument. The red dotted curves are Bessel functions in which the order n is larger than the maximum argument.

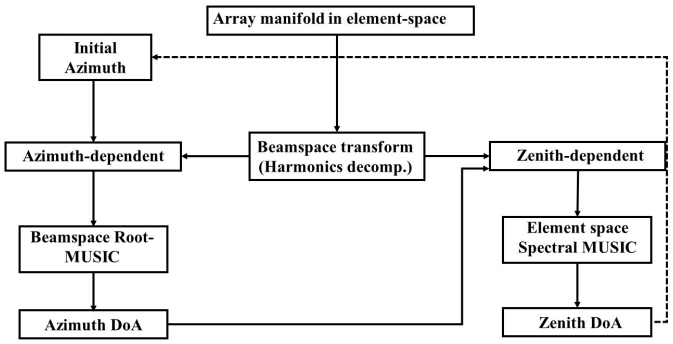

Fig. 3. Our UCA 2-D DoA approach diagram.

may be expressed as an $M \times (2N+1)$ spatial DFT sub-matrix, where each column represents the n-th excitation mode vector $\mathbf{w}_n$, defined as

$$\mathbf{w}_n = \frac{1}{\sqrt{M}}\begin{bmatrix} 1 & \mathrm{e}^{-\mathrm{j}2\pi\frac{n}{M}} & \cdots & \mathrm{e}^{-\mathrm{j}2\pi\frac{n(M-1)}{M}} \end{bmatrix}^{\mathrm{T}}. \tag{8}$$

According to Eq. (7), a good approximation for $\bar{\mathbf{a}}(\phi)$ is

$$\bar{\mathbf{a}}(\phi) = \mathbf{W}^{\mathrm{H}}\mathbf{a}(\phi) \approx \mathbf{J}\mathbf{v}(\mathrm{e}^{\mathrm{j}\phi}), \tag{9}$$

where $\mathbf{v} = [\mathrm{e}^{-\mathrm{j}\phi N} \cdots \mathrm{e}^{-\mathrm{j}\phi}\ 1\ \mathrm{e}^{\mathrm{j}\phi} \cdots \mathrm{e}^{\mathrm{j}\phi N}]^{\mathrm{T}}$, and $\mathbf{J}$ is a diagonal matrix whose elements are $\sqrt{M}j^n J_n(Y\bar{R})$, $-N \le n \le N$. The $(2N+1) \times 1$ beamspace array manifold then becomes

$$\bar{\mathbf{x}}(k) = \mathbf{W}^{\mathrm{H}}\mathbf{A}(\phi)\mathbf{s}(k) + \mathbf{W}^{\mathrm{H}}\mathbf{n}(k) = \bar{\mathbf{A}}(\phi)\mathbf{s}(k) + \bar{\mathbf{n}}(k). \tag{10}$$

Recalling Eq. (2), $\mathbf{R}_{\bar{x}}$ can also be expressed as

$$\mathbf{R}_{\bar{x}} = \mathbf{W}^{\mathrm{H}}\mathbf{R}_x\mathbf{W} = \mathbf{W}^{\mathrm{H}}\mathbf{A}(\phi)\mathbf{R}_s\mathbf{A}^{\mathrm{H}}(\phi)\mathbf{W} + \mathbf{R}_{\bar{n}}. \tag{11}$$

B. Decoupled Spectral MUSIC and Beamspace Root-MUSIC DoA Estimation

The Vandermonde-structured portion of $\bar{\mathbf{a}}(\phi)$, $\mathbf{v}(\mathrm{e}^{\mathrm{j}\phi})$, now allows the use of the Root-MUSIC algorithm, which deals only with azimuthal angle. The zenithal angle, present in $\bar{\mathbf{R}}$, is yet to be dealt with. We can use the simple two-step process for 2-D DoA estimation in Fig. 3. First, the azimuth DoA is estimated via Root-MUSIC, assuming $\theta = 90°$. Then, we perform D 1-D Spectral MUSIC searches through the zenithal angle parameter $\theta \in [0, \pi/2]$. This scheme benefits from the aspects of beamspace Root-MUSIC and solves the problem with reduced computational effort when compared to 2-D Spectral MUSIC.

C. Non-Isotropic Zenith DoA Behavior

The planar geometry of the UCA results in zenithal non-isotropic behavior that affects 2-D DoA. Fig. 4 illustrates these effects on the Absolute DoA Estimation Error (modulus $|\epsilon|$ of the error) for the cases of only Signal of Interest (SoI) and double sources (SoI and Interferer), using the DoA estimation method mentioned in Section II-B.

From this figure, we conclude that the absolute zenith error tends to increase with increasing source zenithal angle while the absolute azimuth error decreases with increasing source zenithal angle, except around the zenith of the interferer, which is set to 50.7 degrees in our experiment. As also seen in Fig. 4, estimation accuracy deteriorates in the two-source case.

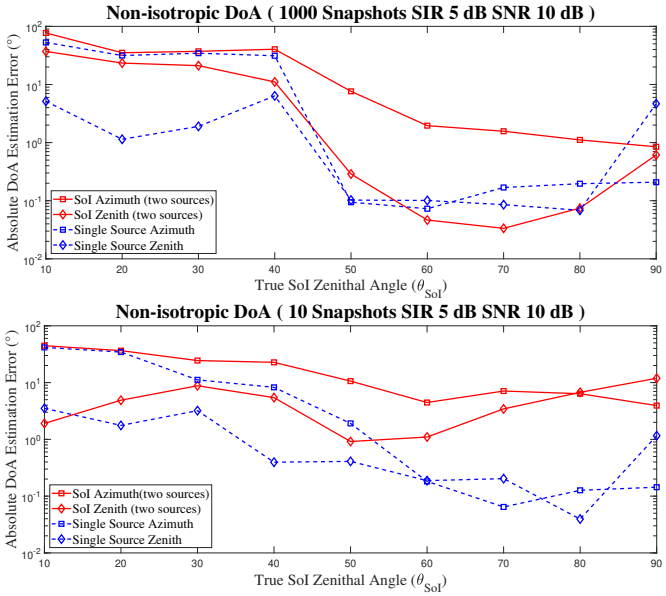

Fig. 4. DoA error of a 16 sensor UCA (mapped in beamspace by 11 phase modes) × zenith for 1 and 2 sources: SoI ($\phi_{SoI} = 37.9°, \theta_{SoI} \in [10°, 90°]$) and interferer ($\phi_{Int} = 120.5°$, and $\theta_{Int} = 50.7°$). 1,000 runs with 1,000 and 10 snapshots, $R = \lambda$, SIR of 3dB, SNR of 5dB. "Az" and "Ze" refers to azimuth and zenith, respectively.

III. DoA Estimation With Reduced Number of Sensors

With a sufficient quantity of sensors for a given radius, each phase mode can be satisfactorily expressed by a single Bessel function of the first kind [14]. For an insufficient number of sensors, Eq. (7) does not hold, and each phase mode is expressed more closely by Eq. (6). Consider a UCA with a reduced number of sensors, $M_{sp} < M$, capable of exciting only $(2N_{sp}+1)$ phase modes, with $N_{sp} = \lfloor M_{sp}/2 \rfloor$. To avoid spatial aliasing, the array needs $(2N+1)$ phase modes to express the receiving characteristics correctly.

The additional $2N - 2N_{sp}$ phase modes can only be incorporated in $\bar{\mathbf{x}}_{sp}(k)$ if each entry $\bar{x}_{n_{sp}}(k)$, $n_{sp} \in [-N_{sp}, \ldots, -1, 0, 1, \ldots, N_{sp}]$, is expressed by more than one phase mode [7], [16]. According to Eq. (6), it is possible to make $l \neq 0$ and express each $\bar{x}_{n_{sp}}(k)$ by as many phase modes as necessary. In this fashion, $(2N+1)$ phase modes are incorporated in $\bar{x}_{n_{sp}}(k)$, even with only $(2N_{sp}+1) < (2N+1)$ entries, each entry expressed by

$$\bar{x}_{n_{sp}}(k) = s(k)\sqrt{M}\left[j^{n_{sp}} J_{n_{sp}}\left(Y\bar{R}\right) \mathrm{e}^{(jn_{sp}\phi)} + j^{\pm(n_{sp}+lM_{sp})} J_{\pm(n_{sp}+lM_{sp})}\left(Y\bar{R}\right) \mathrm{e}^{(\pm j(n_{sp}+lM_{sp})\phi)}\right], \quad (12)$$

with l such that $n_{sp} + lM_{sp} = n$. Such technique is implemented with matrix $\mathbf{H}$ defined as

$$\mathbf{H} = [\mathbf{D}_+ \vdots \mathbf{I} \vdots \mathbf{D}_-], \quad (13)$$

where $\mathbf{I}$ is the $(2N_{sp}+1)$ identity matrix. $\mathbf{D}_+$ is a $(2N_{sp}+1)\times(N-N_{sp})$ matrix of the $(N-N_{sp})$ last columns of $\mathbf{I}$ and $\mathbf{D}_-$ is a $(2N_{sp}+1)\times(N-N_{sp})$ matrix of the $(N-N_{sp})$ first columns of $\mathbf{I}$ when $3N_{sp}+1 > N > N_{sp}$. In [7] we have the form of matrix $\mathbf{H}$ for any values of N and N_{sp} by incorporating additional identity matrices. For example, when $5N_{sp}+1 > N > 3N_{sp}+1$, $\mathbf{H}$ is $[\mathbf{D}_+ \vdots \mathbf{I} \vdots \mathbf{I} \vdots \mathbf{I} \vdots \mathbf{D}_-]$.

As an example, the sparse UCA to be used in Subsection V-A has an aperture that requires $(2N+1) = 11$ phase modes. However, with only 6 sensors, it is capable of exciting only $(2N_{sp}+1) = 5$ modes. Starting with the ideal (theoretical) $(2N+1)$ array manifold $\bar{\mathbf{a}}(\phi)$ and the actual $(2N_{sp}+1)\times 1$ sparse array manifold $\bar{\mathbf{a}}_{sp}(\phi)$ are given by

$$\bar{\mathbf{a}}(\phi) = \left[\mathrm{J}_{-5}, \mathrm{J}_{-4}, \ldots, \mathrm{J}_{-1}, \mathrm{J}_0, \mathrm{J}_1, \ldots, \mathrm{J}_4, \mathrm{J}_5\right]^{\mathrm{T}} \text{ and } \bar{\mathbf{a}}_{sp}(\phi) = \left[\mathrm{J}_{-2}, \mathrm{J}_{-1}, \mathrm{J}_0, \mathrm{J}_1, \mathrm{J}_2\right]^{\mathrm{T}}, \quad (14)$$

where $\mathrm{J}_n = j^n J_n(Y\bar{R})\mathrm{e}^{jn\phi}$. The $(2N_{sp}+1)\times 1$ $\bar{\mathbf{a}}_{ad}(\phi)$, with additional phase modes incorporated, is obtained by

$$\bar{\mathbf{a}}_{ad}(\phi) = \mathbf{H}\bar{\mathbf{a}}_{sp}(\phi) = \Big[(\mathrm{J}_{-2}+\mathrm{J}_3), (\mathrm{J}_{-1}+\mathrm{J}_4), (\mathrm{J}_{-5}+\mathrm{J}_0+\mathrm{J}_5), (\mathrm{J}_1+\mathrm{J}_{-4}), (\mathrm{J}_2+\mathrm{J}_{-3}\Big]^{\mathrm{T}} \quad (15)$$

and $\bar{\mathbf{a}}_{ad}$ replaces $\bar{\mathbf{a}}_{sd}$ as the $(2N_{sp}+1) = 5$ array manifold vector. We can see that, despite having the same dimension $(2N_{sp}+1) = 5$, $\bar{\mathbf{a}}_{ad}(\phi)$ is expressed by $(2N+1) = 11$ phase modes that map the array manifold with improved accuracy, thereby minimizing the effects of insufficient spatial sampling.

IV. DoA Estimation With Small Sample Support

Subspace-based estimation methods are negatively impacted by subspace leakage or loss of orthogonality caused by the small sample support [8], [17], [18]. Next, we briefly review the *S*ubspace Leakage Minimization technique that deals with conditioning the sample covariance matrix via minimizing undesired correlation components. Under reduced number of snapshots K, Eq. (11) can be approximated by

$$\hat{\mathbf{R}}_{\bar{x}} = \mathbf{W}^{\mathrm{H}}\mathbf{A}(\phi)\hat{\mathbf{R}}_s\mathbf{A}^{\mathrm{H}}(\phi)\mathbf{W} + \mathbf{W}^{\mathrm{H}}\hat{\mathbf{R}}_n\mathbf{W} + \hat{\mathbf{T}} + \hat{\mathbf{T}}^{\mathrm{H}}, \quad (16)$$

where $\hat{\mathbf{T}} = \mathbf{A}(\phi)\left[\frac{1}{K}\sum_{k=1}^{K}\hat{\mathbf{s}}(k)\hat{\mathbf{n}}^{\mathrm{H}}(k)\right]$, with $\hat{\mathbf{s}}(k)$ and $\hat{\mathbf{n}}(k)$ being estimates of the signal and noise vectors, respectively.

The first two terms of Eq. (16) are reasonable estimates of $\mathbf{R}_{\bar{x}}$ in Eq. (11) for large K. For smaller K, however, the residual last two cross-correlation terms must be minimized to ensure that $\hat{\mathbf{R}}_{\bar{x}}$ converges to $\mathbf{R}_{\bar{x}}$ [8], as follows. Initially, we utilize $\hat{\mathbf{R}}_{\bar{x}}$ and Root-MUSIC to obtain coarse DoA estimates $\{\phi'_1 \ldots \phi'_D\}$, which are then used to obtain $\mathbf{A}(\phi')$. The estimation of vector $\mathbf{s}(k)$ is carried out from Eq. (10) using a least-squares solution [19] according to [18]

$$\hat{\mathbf{s}}(k) = \left[\mathbf{A}^{\mathrm{H}}(\phi')\mathbf{A}(\phi')\right]^{-1}\mathbf{A}^{\mathrm{H}}(\phi')\mathbf{x}(k), \quad (17)$$

while $\hat{\mathbf{n}}(k) = \mathbf{x}(k) - \mathbf{A}(\phi')\hat{\mathbf{s}}(k)$. Further manipulation of previous results, yields

$$\hat{\mathbf{T}} = \mathbf{P}\hat{\mathbf{R}}_{\bar{x}}\left(\mathbf{I}_{(2N+1)} - \mathbf{P}\right), \quad (18)$$

where $\mathbf{P} = \mathbf{A}(\phi')\left[\mathbf{A}^{\mathrm{H}}(\phi')\mathbf{A}(\phi')\right]^{-1}\mathbf{A}^{\mathrm{H}}(\phi')$ is the estimated signal subspace projector and $\mathbf{I}_{(2N+1)} - \mathbf{P}$ is the respective orthogonal projector. We can then devise an improved version of $\hat{\mathbf{R}}_{\bar{x}}$ based on initial DoAs as

$$\hat{\mathbf{R}}'_{\bar{x}} = \hat{\mathbf{R}}_{\bar{x}} - \mu\left(\hat{\mathbf{T}} + \hat{\mathbf{T}}^{\mathrm{H}}\right),\ \mu \in [0,1]\,. \tag{19}$$

The beamformer and the least-squares solution of $\mathbf{s}(k)$ retain a systematic error, and the residual terms cannot be precisely estimated. We calculate the updated DoAs $\{\phi''_1 \ldots \phi''_D\}$ (the second iteration of DoA estimation) for each discrete increment of μ and choose the optimum value that minimizes the element-space MUSIC spectrum:

$$\mu = \arg\ \min \left\| \sum_{d=1}^{D} \mathbf{a}^{\mathrm{H}}(\mu, \phi''_d)\mathbf{E}_N\mathbf{E}_N^{\mathrm{H}}\mathbf{a}(\mu, \phi''_d) \right\|, \tag{20}$$

where $\mathbf{E}_N$ contains the noise eigenvectors of the autocovariance matrix [20].

V. Numerical Results

This section presents and discusses 2-D DoA estimation simulation results highlighting the effects of the limiting factors and mitigating techniques described herein. We consider two different scenarios, namely *air* and *underwater*. In the later, we assess the UCA behavior in a shallow-water marine environment that includes multipath propagation owing to surface and bottom reflections.

We have shared parameters for both experiments: UCA with radius $R = \lambda$, two narrowband sources with slight zenithal separation, Signal of Interest (SoI) and Interferer with a 3 dB Signal-to-Interference Ratio (SIR), and isotropic AWGN. All results correspond to an average of 1,000 independent runs.

A. Simple Multivariate Evaluations

This subsection shows several UCA 2-D DoA estimations by altering individual limiting parameters (SNR, number of sensors, and quantity of snapshots). In all simulations, the source's angular positions are: SoI with $\phi_{SoI} = 37.9°$, $\theta_{SoI} = 57.7°$, and Interferer with $\phi_{Int} = 120.5°$, $\theta_{Int} = 50.7°$ Subspace leakage results in an unclear definition of

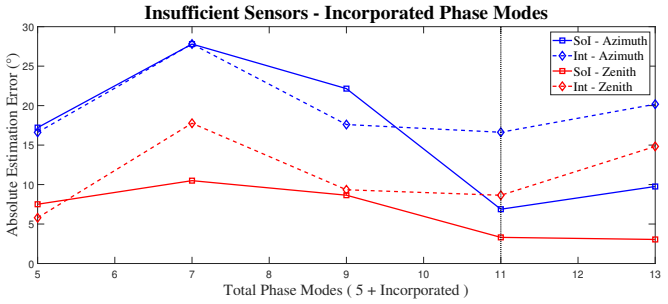

Fig. 5. Incorporated phase modes in 2-D DoA estimation. UCA having **six sensors** with a spacing of 1.047λ, resolving **a single** (above) and **two** (below) narrowband source with angular positions $\phi_{SoI} = 37.9°$ and $\theta_{SoI} = 57.7°$. SNR of 10 dB and sample support of 1,000 snapshots. Additional phase modes are incorporated (from an initial 5 up to a total of 13). The vertical dotted line indicates the optimum number of phase modes.

signal and noise eigenvectors and difficulties in sorting signal eigenvectors by magnitude. Leakage Minimization addresses this problem and is dependent of the factor μ in order to estimate and reduce cross-correlation components, mitigating subspace leakage. In Fig. 6 we can see the effects of the factor μ in the mitigation of the small sample support problem and the selection of the value utilized in previous results.

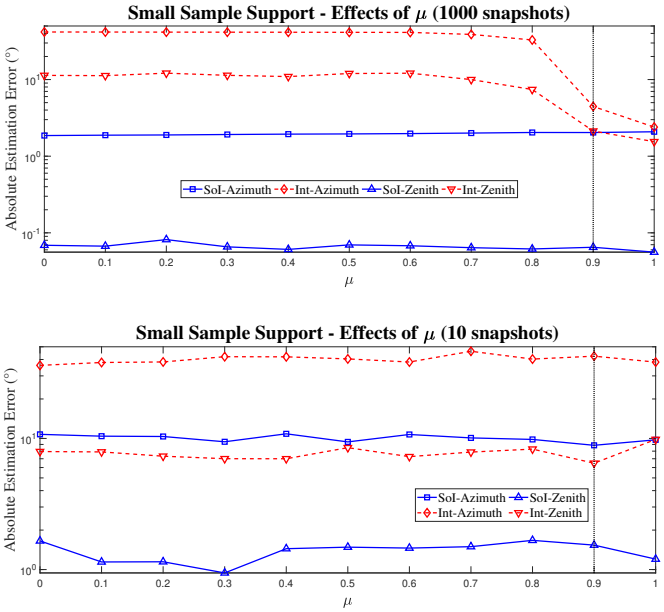

Fig. 6. Effects of factor μ in small sample support UCA 2-D DoA. 16 sensor UCA mapped by 11 phase modes. Resolving two narrowband sources with angular positions $\phi_{SoI} = 37.9°$, $\theta_{SoI} = 57.7°$, $\phi_{Int} = 120.5°$ and $\theta_{Int} = 50.7°$. SNR 10 dB and SIR 3 dB. Sample support **1,000 and 10 snapshots**.

For the case of a limited number of sensors, we used a sample support of 1,000 snapshots. The UCA has only six sensors with a spacing of 1.047λ, resulting in spatial aliasing. Only 5 phase modes ($N = 2$) map the thinned array; however, as shown in Fig. 5, incorporating additional phase modes—up to 11—considerably improves the estimations. For the case of small sample support, the UCA has 16 sensors, mapped in beamspace by 13 phase modes ($N = 6$) and with element spacing of 0.393λ. Sample support ranges from 100 to single snapshots and $\mu = 0.8$.

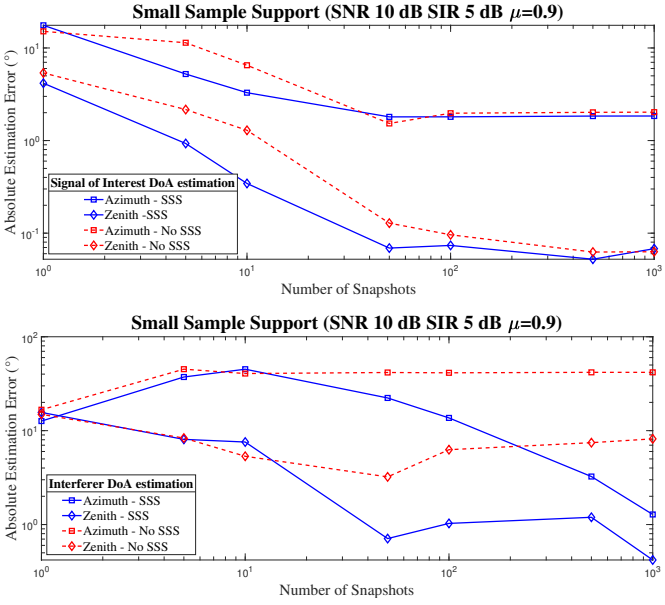

Fig. 7. Decreasing sample support in UCA 2-D DoA. **SoI** (above), **Interferer** (below) estimation errors as a function of the number of snapshots in the presence (SSS) and absence (no SSS) of small sample support mitigation. UCA with 16 sensors mapped by 11 phase modes. Narrowband source with angular positions $\phi_{SoI} = 37.9°$, $\theta_{SoI} = 57.7°$. **SIR of 5 dB and SNR of 10 dB**. μ of 0.9.

Fig. 7 depicts the influence of decreasing sample support, where the plots with SSS indicate the use of small sample

support mitigation. The absolute error increases with the reduction of snapshots. Both techniques (additional phase modes and matrix conditioning) can improve solutions and even extend the lower limits of sample support where DoAs can be accurately estimated.

B. Simultaneous Spatial And Temporal Evaluations

In this section, we address the problems of reduced spatial and temporal sampling simultaneously. Employing combined phase mode incorporation and Leakage Minimization techniques, we evaluate their joint behavior similarly to the isolated multivariate simulations.

The specific parameters for these simulations are: an ensemble of 1.000 independent runs, sources with a SIR of 3 dB, and AWGN with an SNR of 10 dB. Six sensors UCA mapped in beamspace by 5, and up to 13, phase modes. Leakage Minimization μ factor of 0.8 and sample support ranging from 1.000 to 5 snapshots. Angular positions are the same as in Section V-A.

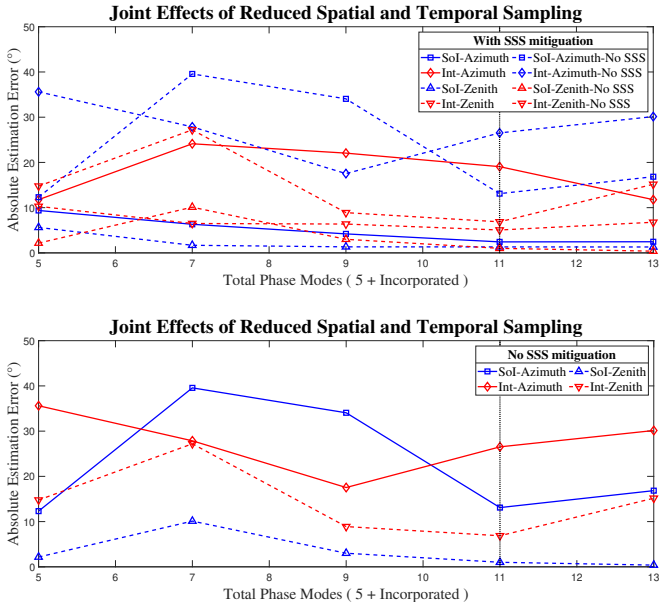

Fig. 8. Combined effects of incorporating phase modes in small sample support 2-D DoA estimation **employing Leakage Minimization** (above) and **without Leakage Minimization** (below). UCA having **six sensors** with spacing of 1.047λ, resolving **two** narrowband sources with angular positions $\phi_{SoI} = 37.9°$, $\theta_{SoI} = 57.7°$, $\phi_{Int} = 120.5°$ and $\theta_{Int} = 50.7°$. SIR of 3 dB, SNR of 10 dB and small sample support of **10 snapshots**. Additional **phase modes are incorporated** (from an initial 5 up to a total of 13).

Starting with a more detailed analysis of the number of phase modes for beamspace mapping, we show the effects of incorporating phase modes to a small sample support 2-D DoA estimation, both in the presence and absence of Leakage Minimization. Fig. 8 depicts increasing incorporated phase modes solution errors for estimations with only 10 snapshots.

Continuing, with a greater focus on small sample support, Fig. 9 depict the combined behavior of beamspace mapping, by 5 and 11 phase modes, and Leakage Minimization for decreasing sample support.

The combined results tend to behave similarly to the individual mitigating techniques results in Section V-A, where additional phase modes yield better results in spatially aliased solutions and minimized leakage solutions yield better results than small sample support solutions.

However, we can observe that, for the combined limiting factors scenario, leakage minimization contributions for the overall improvements are somewhat more pronounced, especially for the Interferer DoA solutions. This behavior can be seen in Fig. 9, where the spatially aliased, leakage minimized solutions can be better than solutions with incorporated phase modes but without leakage minimization. These observations also point to mutual interference of the two mitigating techniques (phase modes incorporation and leakage minimization), as these techniques are based on different principles to improve DoA estimation.

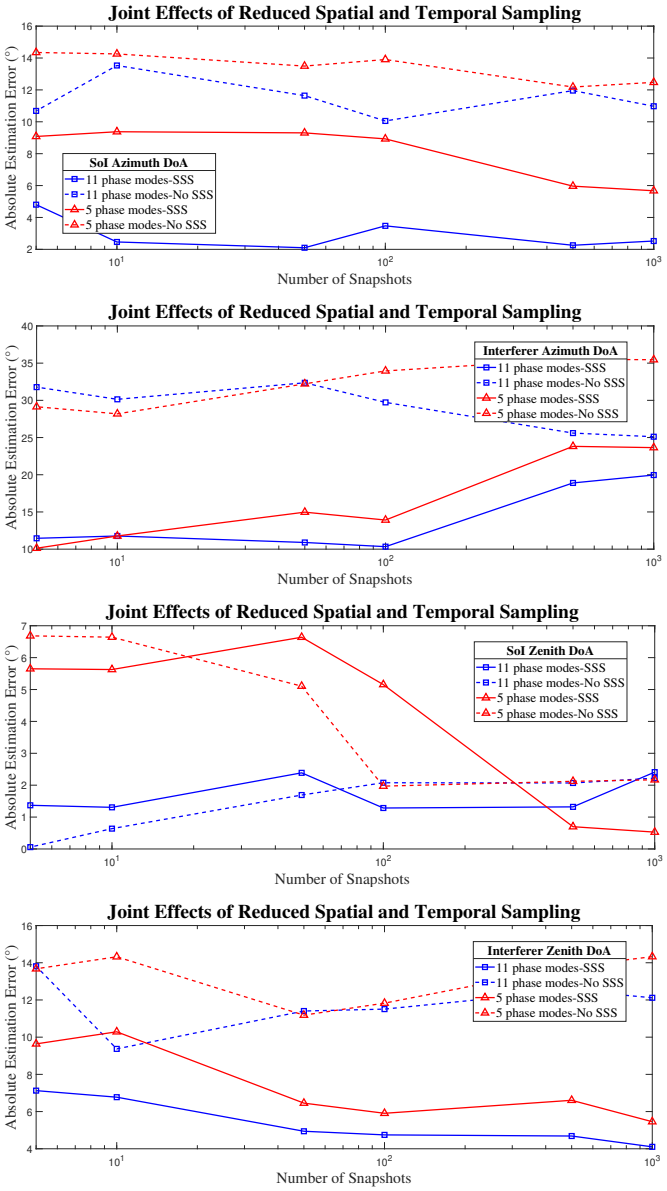

Fig. 9. Combined behavior of beamspace mapping and Leakage Minimization with decreasing sample support for **azimuth** (above) and **zenith** (below) DoAs of **SoI** and **Interferer**. UCA has **six sensors** with a spacing of 1.047λ and beamspace mapping with 5 and 11 (5+6 incorporated) phase modes. Resolving **two** narrowband sources with angular positions $\phi_{SoI} = 37.9°$, $\theta_{SoI} = 57.7°$, $\phi_{Int} = 120.5°$ and $\theta_{Int} = 50.7°$. SIR of 3 dB and SNR of 10 dB.

C. Underwater Environment Simulation

This subsection employs the methods described herein in conditions similar to a real shallow underwater scenario. We

utilize real-life signals from the samples database of ShipsEar, available in http://atlanttic.uvigo.es/underwaternoise/. We assume two surface sources, namely a cruise ship and a motorboat, immersed in isotropic AWGN with SNR of 15dB and simulate the effects of surface and bottom reflections, resulting in multipath propagation.

The submerged UCA has 32 sensors mapped by 15 phase modes ($N = 7$), $R = \lambda$ and the central frequency was set to 1 kHz. Sources' angular position are cruise ship (SoI) $\phi_{CS} = 23.1°$, $\theta_{CS} = 48.5°$ and motorboat (Interferer) with $\phi_{MB} = 142°$, $\theta_{MB} = 34.7°$, and SIR of 5dB. Their respective multipath spurious signals are hitting the array from $\phi_{CSmulti} = 26°$, $\theta_{CSmulti} = 19.3°$, and $\phi_{MBmulti} = 143.9°$, $\theta_{MBmulti} = 11.5°$. These spurious multipath DoAs represent surface reflections and slight azimuthal refraction. Spurious multipath sources have an attenuation of 15dB.

Despite the unattended problem of correlated sources, results depicted in Fig. 10 show that the leakage minimization technique, indicated by SSS in the legend, improved results, mainly with Root-MUSIC azimuth estimation. Also, using a single value of μ for a wide range of sample support may have different and even contradictory effects.

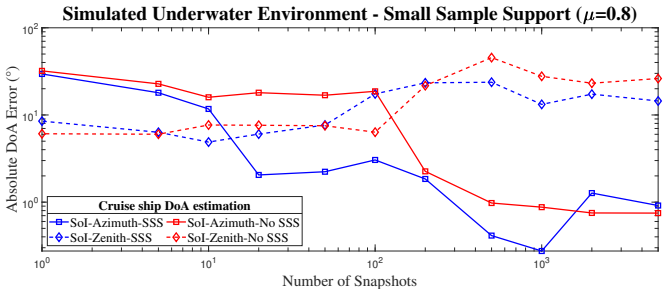

Fig. 10. The influence of decreasing sample support in 2-D DoA of two sources with simulated underwater multipath propagation.

VI. Conclusion and Final Remarks

This paper shows that reduced spatial sampling and inaccurate beamspace mapping effects can be satisfactorily mitigated by incorporating additional phase modes. We observed that matrix conditioning could mitigate biased covariance matrices, allowing even a single snapshot DoA estimation. In the underwater environment simulation, the effects of multipath, akin to correlated sources, are present. Although not within the scope of this work, the mitigation techniques addressed herein applied to correlated sources in a small sample support situation yielded favorable results.

Our results show that the azimuthal DoA (estimated with Root-MUSIC) suffers more from the reduced number of sensors and small sample support than the zenithal DoA (estimated with Spectral MUSIC). The methods and results of this work indicate reduced estimation speeds, due to simplified computations, and good accuracy even when employing several techniques simultaneously and with real-life broadband signals. These attributes can be particularly suited, for example, for 360° coverage phased array for broadband passive detection and tracking, such as Electronic Warfare equipment or Cylindrical Hydrophone Arrays (CHA) aboard surface vessels and submarines.

References

[1] A. W. Rudge, *The Handbook of Antenna Design*. London: P. Peregrinus on behalf of the Institution of Electrical Engineers, 1982, vol. II.

[2] H. L. Van Trees, *Optimum Array Processing*, 2nd ed., ser. Detection, Estimation and Modulation Theory. 605 Third Avenue, New York, NY 10158-0012: John Wiley and Sons, Ltd, 2007, vol. IV.

[3] H. Krim and M. Viberg, "Two decades of array signal processing research: the parametric approach," *IEEE Signal Processing Magazine*, vol. 13, no. 4, pp. 67–94, 1996.

[4] V. Krishnaveni, T. Kesavamurthy, and Aparna. B, "Beamforming for Direction-of-Arrival (DOA) Estimation-A Survey," *International Journal of Computer Applications*, vol. 61, pp. 4–11, 01 2013.

[5] C. E. Hickman, H. P. Neff, and J. D. Tillman, "The theory of a single-ring circular antenna array," *Transactions of the American Institute of Electrical Engineers, Part I: Communication and Electronics*, vol. 80, no. 2, pp. 110–115, 1961.

[6] I. Longstaff, P. Chow, and D. Davies, "Directional properties of circular arrays," *Proceedings of the Institution of Electrical Engineers*, vol. 114, pp. 713–718(5), June 1967.

[7] R. Goossens, H. Rogier, and S. Werbrouck, "UCA Root-MUSIC with sparse uniform circular arrays," *IEEE Transactions on Signal Processing*, vol. 56, no. 8, pp. 4095–4099, 2008.

[8] M. Shaghaghi and S. A. Vorobyov, "Subspace leakage analysis and improved DOA estimation with small sample size," *IEEE Transactions on Signal Processing*, vol. 63, no. 12, pp. 3251–3265, 2015.

[9] W. Hong and A. Tewfik, "On the application of uniform linear array bearing estimation techniques to uniform circular array," in *Antennas and Propagation Society Symposium 1991 Digest*, 1991, pp. 372–375 vol.1.

[10] R. Schmidt, "Multiple emitter location and signal parameter estimation," *IEEE Transactions on Antennas and Propagation*, vol. 34, no. 3, pp. 276–280, 1986.

[11] M. Zoltowski, G. Kautz, and S. Silverstein, "Beamspace Root-MUSIC," *IEEE Transactions on Signal Processing*, vol. 41, no. 1, pp. 344–364, 1993.

[12] T. Akiyama, T. Yamaoka, and N. Hamada, "2-D angle estimation using the constrained MUSIC with circular array," in *ISSPA '99. Proceedings of the Fifth International Symposium on Signal Processing and its Applications (IEEE Cat. No.99EX359)*, vol. 2, 1999, pp. 877–880.

[13] M. Abramowitz and I. A. Stegun, *Handbook of Mathematical Functions*. New York: Dover Publications, 1964.

[14] M. Wax and J. Sheinvald, "Direction finding of coherent signals via spatial smoothing for uniform circular arrays," *IEEE Transactions on Antennas and Propagation*, vol. 42, no. 5, pp. 613–620, 1994.

[15] C. Mathews and M. Zoltowski, "Eigenstructure techniques for 2-D angle estimation with uniform circular arrays," *IEEE Transactions on Signal Processing*, vol. 42, no. 9, pp. 2395–2407, 1994.

[16] S. Li and H. Chen, "A novel method of DOA estimation on sparse uniform circular array," in *2016 CIE International Conference on Radar (RADAR)*, 2016, pp. 1–4.

[17] L. Xingxing, W. Dangwei, X. Ma, and Z. Chang, "Robust adaptive beamforming algorithm in the situation of small sample size," in *2016 CIE International Conference on Radar (RADAR)*, 2016, pp. 1–4.

[18] F. Wen and Z. Wang, "An efficient two-step direction finding method in sample-starved environments," in *2017 20th International Conference on Information Fusion (Fusion)*, 2017, pp. 1–5.

[19] L. Trefethen and D. Bau, *Numerical Linear Algebra*. 3600 Market Street, Floor 6, Philadelphia, PA 19104: Society for Industrial and Applied Mathematics (SIAM), 1997.

[20] G. Jiang, X. Mao, and Y. Liu, "Direction-of-arrival estimation for uniform circular arrays under small sample size," *Journal of Systems Engineering and Electronics*, vol. 27, no. 6, pp. 1142–1150, 2016.